



Article

Effect of Al₂O₃ Dot Patterning on CZTSSe Solar Cell Characteristics

Se-Yun Kim^{1,2}, Sanghun Hong³, Seung-Hyun Kim¹, Dae-Ho Son^{1,4}, Young-Ill Kim¹, Sammi Kim¹, Young-Woo Heo³, Jin-Kyu Kang^{1,4,*}  and Dae-Hwan Kim^{1,4,*} 

¹ Research Center for Thin Film Solar Cells, Daegu-Gyeongbuk Institute of Science and Technology (DGIST), Daegu 42988, Korea; kimseyun@kyungnam.ac.kr (S.-Y.K.); seunghyun@dgist.ac.kr (S.-H.K.); dhson@dgist.ac.kr (D.-H.S.); lynx012@dgist.ac.kr (Y.-I.K.); smkim@dgist.ac.kr (S.K.)

² Department of Nano Materials Science and Engineering, Kyungnam University, Gyeongsangnam-do 51767, Korea

³ School of Materials Science and Engineering, Kyungpook National University, Daegu 41566, Korea; shhong@dgist.ac.kr (S.H.); ywheo@knu.ac.kr (Y.-W.H.)

⁴ Division of Energy Technology, Daegu-Gyeongbuk Institute of Science and Technology (DGIST), Daegu 42988, Korea

* Correspondence: apollon@dgist.ac.kr (J.-K.K.); monolith@dgist.ac.kr (D.-H.K.)

Received: 31 July 2020; Accepted: 17 September 2020; Published: 18 September 2020



Abstract: In this study, a 5-nm thick Al₂O₃ layer was patterned onto the Mo electrode in the form of a dot to produce a local rear contact, which looked at the effects of this contact structure on Cu₂ZnSn(S_{1-x}Se_x)₄ (CZTSSe) growth and solar cell devices. Mo was partially exposed through open holes having a square dot shape, and the closed-ratios of Al₂O₃ passivated areas were 56%, 75%, and 84%. The process of synthesizing CZTSSe is the same as that of the previous process showing 12.62% efficiency. When the 5-nm-Al₂O₃ dot patterning was applied to the Mo surface, we observed that the MoS₂ formation was well suppressed under the area coated of 5-nm-Al₂O₃ film. The self-alignment phenomenon was observed in the back-contact area. CZTSSe was easily formed in the Mo-exposed area, while voids were formed near the Al₂O₃-coated area. The efficiency of the CZTSSe solar cell decreased when the Al₂O₃ passivated area increased. The exposure area and pitch of Mo, the collecting path of the hole, and the supplying path of Na seemed to be related to efficiency. Thus, it was suggested that the optimization of the Mo-exposed pattern and the additional Na supply are necessary to develop the optimum self-aligned CZTSSe light absorber.

Keywords: CZTSSe; metal precursor; two-step process; back-contact passivation; void arrangement

1. Introduction

The efficiencies of CdTe and CIGS solar cells are reported to be close to those of Si solar cells, at 22.1% and 23.4%, respectively [1]. Unlike Si thin-film solar cells, CdTe and CIGS materials have a significant light absorption coefficient. They can thus absorb light sufficiently in thin films for solar cells [2]. Therefore, CdTe and CIGS thin-film solar cells are the most likely candidates to be applied to building-integrated photovoltaics (BIPVs) and vehicle-integrated photovoltaics (VIPVs) as flexible solar cells. However, because CdTe and CIGS materials have problems of Cd toxicity and supply and demand instability due to the scarcity of In and Ga, it is necessary to develop solar cells using abundant, non-toxic materials with no stability issues. As one of the emerging solar cell materials, halide perovskite materials have shown excellent characteristics [1,2]. Even so, there continue to be doubts about halide perovskite materials' potential for commercialization due to photo, humidity, and thermal stability issues [3–7]. Another promising material is CZTSSe, which is a non-toxic and abundant material with high absorption coefficient [1,8,9]. Unfortunately, unlike CIGS, CZTSSe has

not overcome the 12.6% efficiency barrier achieved in 2013 by the hydrazine solution process [10]. The origin of the barrier was estimated as follows: 1) Cu + Zn disordered kesterite has the lowest formation energy, causing additional problems such as energy bandgap fluctuation and a large amount of defect formation [11–13]. 2) The highly stable ZnS(e) phase [14,15], which always participates in the reaction pathway [16], makes it difficult to form a CZTSSe layer with a uniform composition. SnZn, which is a killing defect, is well-formed at conditions of Zn-poor kesterite [17–19]. 3) The Sn multivalent state is easily formed at a low partial pressure of chalcogenide [18,20]. 4) SnS loss occurs during the cooling process by CZTSSe decomposition at high temperatures [21,22].

Recently, it has been reported that the solar cell characteristics of CZTSSe synthesized using metal precursors exhibit high efficiency [15,23–28]. Our group has tied the record of the world's highest efficiency using H₂S gas and Se pellets. [23]. Since our process was performed at relatively high Se pressures and low temperatures, we believe that the impact on problems 3) and 4) has been reduced. According to our CZTSSe synthesis process, which shows efficiency of 12.62%, the CZTSSe absorption layer has the following unique microstructure. A CZTSSe double layer consisting of a dense upper CZTSSe layer and bottom CZTSSe layer that is partially composed of voids. [15]. Moreover, between the upper CZTSSe and bottom CZTSSe, the ZnSSe secondary phase remains as an unreacted residue [15]. Cu- and Cu-Sn-SSe secondary phases are distributed in the Mo back contact region [15]. According to the results of the formation mechanism investigation of the Cu- and Cu-Sn-SSe phases in the Mo-back contact region, the secondary phase formation can be suppressed by controlling the wetting characteristic of the Mo-back contact side [29]. When the Al₂O₃ coated Mo/SLG substrate is used, the formation of the secondary phase distributed at the Mo back contact region is completely suppressed [29]. However, void formation at the bottom CZTSSe layer of the CZTSSe double layer is inevitable when using Sn/Cu/Zn metal precursors [15,23–26]. Further experiments have shown that using a 130-nm sputtered Al₂O₃ line patterned Mo / SLG substrate, voids present in the bottom CZTSSe layer could be arranged in the Al₂O₃ coated area while the bottom CZTSSe was arranged on the Mo exposed area [26]. In previous studies, one type of line pattern was applied and MoSSe formation control was not performed [26]. Nevertheless, it was meaningful for the first time to show the possibility of arranging the irregular distribution of the bottom CZTSSe as desired.

In this study, a 5-nm-Al₂O₃ layer was deposited on the Mo electrode to suppress the MoSSe formation perfectly. By changing the distribution of square dots of the same size, the open ratio was changed to 44%, 25%, and 16%, and the passivation ratios were 56, 75, and 85%. Sizing of the Mo-exposed dot and the distance between each dot was designed based on the ratio of void and size of the bottom CZTSSe in the previous study. Mo-exposed square dots were formed by the photolithography process to control the distribution of the bottom CZTSSe. The effects of the passivated emitter and rear cell (PERC) and defect passivation at back contact side may be caused by Al₂O₃ intermediate layer, which may increase the cell efficiency [30–32]. In the case of solar cell characteristics, as the Al₂O₃ coated area increased, the efficiency decreased. The origin of reduced cell efficiency depends on the 5-nm-Al₂O₃ dot patterning distribution, which was speculated to be due to the insufficient diffusion of Na from SLG and non-optimized patterning for collecting the photo-generated carrier.

2. Materials and Methods

A BOE solution etched the Mo-deposited SLG substrate, and a 5-nm-thickness Al₂O₃ layer was deposited using ALD. In order to form the dot pattern, the general photolithography process was conducted using a photo-mask. The Sn (275 nm)/Cu (160 nm)/Zn (188 nm)/Mo stacked metal precursors for the CZTSSe absorber layer were deposited using 99.99% pure Sn, Cu, and Zn sputtering targets. A quartz box was used for the sulfo-selenization process with a SiC-coated graphite holder as the sample holder. Several Se shots (0.2 g, Sigma-Aldrich, Inc. St. Louis, United States) were placed on the quartz boat's bottom, and the graphite holder was placed in the quartz box. The vaporized Se source flowed into the sample through the holes that were designed on four sides of the SiC-coated graphite

holder. H₂S (250 sccm) and Ar (2000 sccm) gas were supplied until the chamber pressure reached 700 Torr. The sample was heated at 300 °C for 15 min and then heated to 480 °C for 10 min.

A 50-nm-thick CdS buffer layer was deposited by chemical bath deposition. RF-sputtering deposited the intrinsic 50-nm-thick ZnO layer and 300-nm-thick Al-doped ZnO layer. Finally, a 20-nm-thick Ni and 2- μ m-thick Al grid were deposited via e-beam evaporation.

The microstructure of the CZTSSe layer was characterized by FESEM (Hitachi, SU8020, Tokyo, Japan). The depth profile of each component of CZTSSe was analyzed by TOF-SIMS (ION TOF, TOF-SIMS 5-100, Heisenbergstraße, Germany). The solar cells were characterized according to the 1.5 AM illuminated J–V characteristics (94022A solar simulator Newport Co., Keithley 4200 semiconductor characterization system, Berkshire, United Kingdom) in our laboratory.

3. Results

Through applying the photolithography process, the effect of the 5-nm- Al₂O₃ dot patterning distribution on the CZTSSe solar cell efficiency was investigated, as shown in Figure 1a. Since MoOx forms easily, etching by the BOE solution was first conducted. As a result, the wetting angle (contact angle) of the droplet on the BOE-etched Mo surface ranged from 16.64° to 12.23°, as shown in Figure S1. And then, the 5-nm-thickness Al₂O₃ layer is deposited using ALD; the wetting angle of the droplet on the 5-nm-Al₂O₃ coated Mo surface is observed as 27.07°. Then, the general photolithography process is conducted to make the patterning in order as shown in Figure 1a. The following were conducted in order: Photoresistor coating, exposure using photo-mask, development for the patterning of the photoresistor, etching of the 5-nm-Al₂O₃ layer, and finally stripping the photoresistor. Photographs of the patterned 5-nm-Al₂O₃ coated Mo substrates are shown in Figure 1b with its photo-mask design. The patterning by photolithography is rough, owing to the poor resolution of the development process. However, the passivated-ratio trends can be expected by the photo-mask; the passivated-ratio of the photo-masks is 56, 75, and 84%, respectively.

Figure 1c–f show FESEM images of the CZTSSe samples using substrates with 75% 5-nm-Al₂O₃ passivated-area. FESEM images of the CZTSSe samples using substrates with 56% 5-nm-Al₂O₃ passivated-area are shown in Figure S2. Figure 1c shows the CZTSSe top view. Compared with samples without 5-nm-Al₂O₃ patterning, the relatively upper surface morphology appears to be flattened. A previous study found that when large voids were formed in the bottom CZTSSe layer, the grain size of the upper CZTSSe formed on the top was small, and the thickness was thin [33]. When large voids were not formed in the bottom CZTSSe layer, the grain size of the upper CZTSSe formed on the top was large and thick [33]. Hence, when Sn/Cu/Zn/Mo stacked precursor was used to synthesize the CZTSSe film, the fluctuating morphology of the CZTSSe film was formed. However, when the Sn/Cu/Zn/Al₂O₃/Mo stacked precursor was used to synthesize the CZTSSe film, the flat morphology of the CZTSSe film was observed. These results may have been affected by the regular arrangement of voids. The CZTSSe layer was lifted off using epoxy to confirm the distribution of bottom CZTSSe; this method is shown in Figure S3. Figure 1d shows the Al₂O₃ patterned Mo surface microstructure remaining after exfoliation. CZTSSe layer delamination appears to occur at the CZTSSe/Al₂O₃ interface or the upper CZTSSe/bottom CZTSSe interface, as shown in Figure 1d. Figure 1e,f shows a cross-sectional FESEM image. MoSSe growth appears to occur only in the Mo-exposed area and seems to completely inhibit MoSSe growth in the region where 5-nm Al₂O₃ is passivated. Also, although the bottom CZTSSe is arranged in the Mo-exposed area, an area in which the bottom CZTSSe exists in the Al₂O₃ coated area is sometimes found. It was confirmed that the bottom CZTSSe is well connected to the Mo-exposed area in a dot pattern, and the growth of MoSSe was well suppressed through the 5-nm-Al₂O₃ layer.

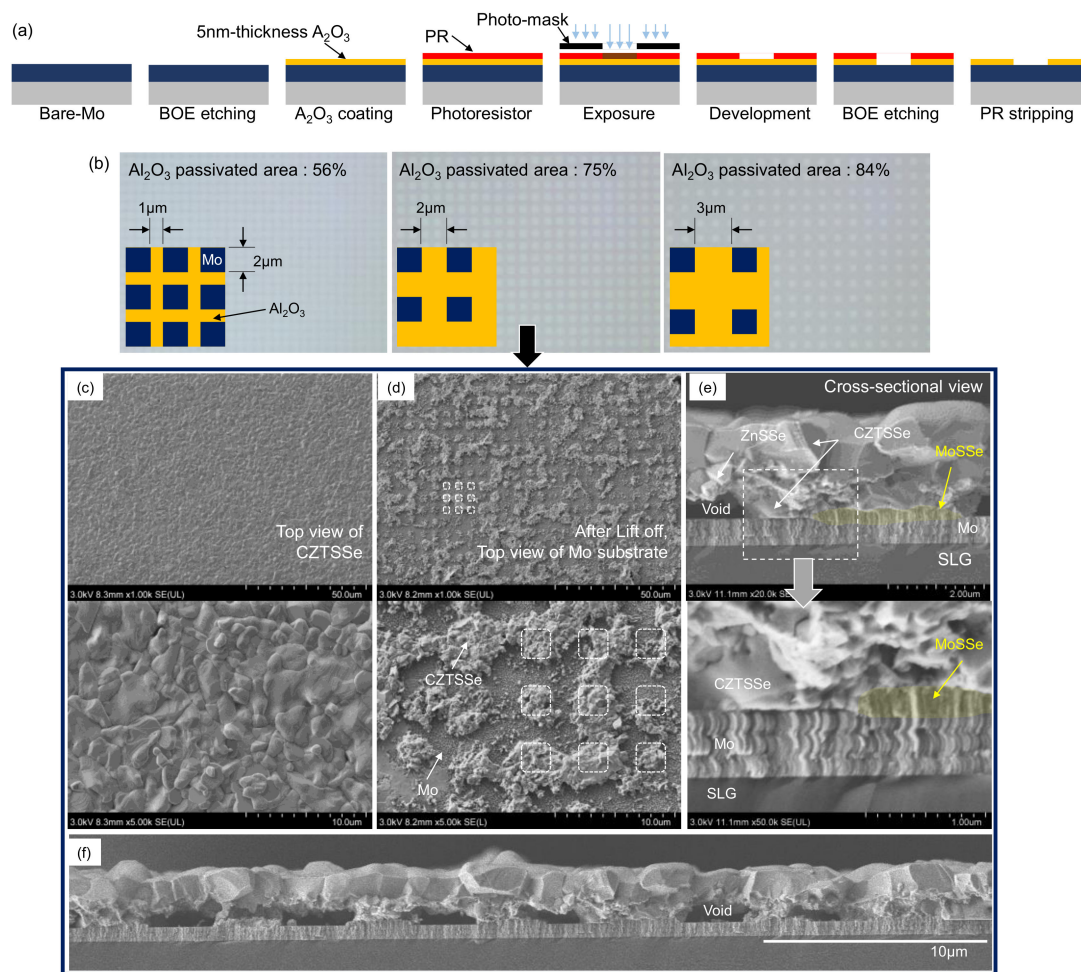


Figure 1. (a) Sequence of Al_2O_3 dot patterning by the photolithography process. (b) Photographs of the dot-patterned $\text{Al}_2\text{O}_3/\text{Mo}$ substrate and its photo-mask pattern (Al_2O_3 passivated ratio is 56, 75, and 84%, respectively). FESEM images of (c) top view, (d) top view of Mo substrate after lifted-off, and (e) and (f) cross-sectional view of a sample with a passivation area of 75%.

Using a series of 5-nm- Al_2O_3 coated Mo substrates, the CZTSSe solar cells were fabricated and characterized, as shown in Figure 2 and Table 1. It was observed that the efficiency decreases because J_{sc} decreases with the Al_2O_3 passivated area. FF tended to decrease slightly, and V_{oc} changes according to the passivation area were insignificant. Due to the nature of our CZTS fabrication process, the absorber layer without patterning is expected to be in direct contact with Mo only about 50–60% of the CZTSSe lower part [15]; the remaining about 40–50% have voids unevenly distributed at the CZTSSe/Mo interface [15]. As shown in Table 1, the effect of increasing V_{oc} due to the back-contact passivation seems to be insignificant (for reference, the dispersion range of V_{oc} value within the same CZTSSe sample in our laboratory is about ~ 0.01 V). This may be because many voids still exist between the Al_2O_3 and the absorption layer, and thus the passivation by Al_2O_3 was not well performed. When the passivated area increased, the FF tend to decrease. It may be due to insufficient back contact formation. If all the 16% areas exposed to Mo serve as CZTS contacts, there will be no big problem (normally, in the case of CIGS, the passivation area is set up to the 95% level [34]). However, in the case of CZTS, since the Zn-related secondary phase may exist between upper CZTSSe and lower CZTSSe, it may interfere with the current flow. If the contact area is small, the degree of interference will be large. When the contact area initially provided is 16% (84% passivated device), it is estimated that the presence of the Zn-related secondary phase interferes with the role of the contact, resulting in a significant reduction in FF. The decrease in J_{sc} is likely to be due to changes in the electro-optical properties of the film such

as average composition, local composition, crystallinity, thickness fluctuation, and surface morphology (reflectivity). The above characteristic changes are related with Na diffusion [35–43]. It was thought that sufficient Na diffusion did not occur through the Al₂O₃ intermediate layer. Thus, the distribution of Na composition in the CZTSSe layers was analyzed by TOF-SIMS.

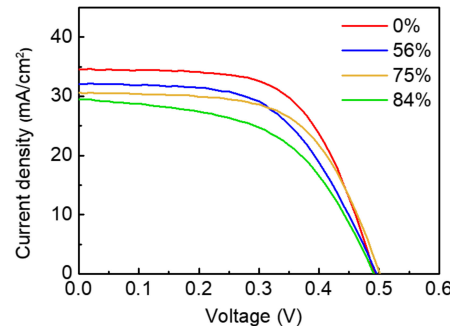


Figure 2. I–V curves of the best efficiency of the CZTSSe cell device, coated with different passivation ratios.

Table 1. Open circuit voltage (Voc), short-circuit current density (Jsc), Fill Factor (FF), and power conversion efficiency (Eff) of the CZTSSe devices fabricated with different closed-ratios of Al₂O₃ passivated areas.

Al ₂ O ₃ Passivated Area (%)	Voc [V]	Jsc [mA/cm ²]	FF [%]	Eff [%]
0	0.493	34.58	61.22	10.43
56	0.496	32.09	56.16	8.94
75	0.502	30.61	60.37	9.27
84	0.492	29.54	52.82	7.67

As shown in Figure 3, the intensity of Na composition in the CZTSSe layer of the fully open cell is strongest, and the intensity of the Na decreases when the 5-nm-Al₂O₃ passivated area increases. The full TOF-SIMS spectrums of CZTSSe devices are found in Figure S4. So far, there have been reports about the effect of Na on the formation of high-quality CZTSSe. In CZTSSe, it has been reported that Na affects grain growth [35–37], defect passivation [38–40], increase in the p-type carrier concentration [41], prolonging the lifetime of the photo-generated carrier [42], and the reduction of non-radiative recombination [42,43]. However, the results of our TOF-SIMS analysis show that the amount of Na present in the CZTSSe absorber layer decreases with increasing Al₂O₃ passivated-area. In the results of CIGS solar cells, it was reported that when Na was not sufficiently diffused by Al₂O₃ patterning, FF and Voc decreased, and this tendency was improved by adding NaF [30,34,44]. In general, when using Al₂O₃ as an intermediate layer in the field of CIGS, it is known that Voc, Jsc, and FF increase for the following reasons. 1) The interface’s defect passivation effect is observed when the Al₂O₃ interlayer is applied to the CIGS/Mo interface [31,44]. 2) The passivated emitter and rear cell (PERC) effect applied to Si solar cells were expected by applying the Al₂O₃ layer to the CIGS/Mo interface in CIGS solar cells [30,31]. This negative charge reflection effect is expected to play an important role in addition to the band grading effect [31]. 3) Research has been conducted to collect the gain by the light reflectance effect in thin CIGS by inserting MgF₂ into the intermediate layer together with Al₂O₃ [45]. Similarly, in CZTSSe solar cells, it has also been reported that the effect of interface defect passivation occurs when Al₂O₃ is applied to the void-free CZTSSe layer, increasing Jsc, Voc, and FF [32]. The following points should be considered to maximize the Al₂O₃ interlayer passivation effect. All of these Al₂O₃ interlayers need open points for the photo-generated holes to escape. Patterning for open points is known to require design based on the diffusion length, which derives the carrier lifetime in the light absorption layer. For example, in some cases, the pattern design of the back-contact

passivation was decided based on the diffusion length of the minor carrier [34]. In these cases, the opening size was about a quarter of the diffusion length of the minor carrier, and the distance of the dot to the dot was designed to be twice as long as the diffusion length of the minor carrier [34]. The reason that the diameter and distance are given in a specific ratio is presumably to prevent minor carriers from acting as leakage currents. The carrier lifetime of photo-generated carriers obtained from TRPL analysis in CZTSSe is excitation-intensity-dependent, voltage-dependent, and temperature-dependent [46,47]. In addition, carrier trapping, surface effects, and energetic relaxation of carriers are generally involved in PL transitions, making it difficult to define carrier lifetime simply [46,47]. The diffusion length of CZTS derived from the photo-Hall effect is reported to be 0.75–1.5 μm [48]. Based on the reported diffusion length, the suitable dot diameter might be and the distance between dots might be 200–400 nm, and 1.5–3 μm respectively. Our patterning design has a small line width that is at the limit of the general aligner but, referring to the above, it is necessary to reduce both the dot size and distance between the dots further. To design such a pattern, it is required to use a stepper or e-beam lithography process, which is more advanced than the current equipment.

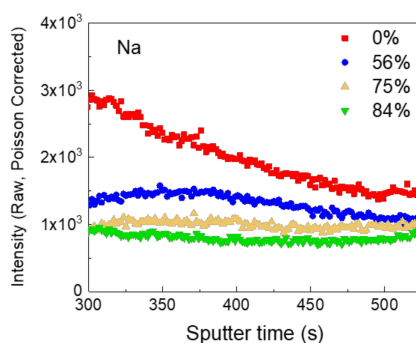


Figure 3. TOF-SIMS depth-profile of Na in the CZTSSe layer parts in the solar cell device, was coated with different passivation ratios.

Our results that bottom CZTSSe of the CZTSSe double layer can be aligned by the patterning of the Al_2O_3 intermediate layer show the possibility of effectively solving the problems found in CZTSSe synthesized using conventional metal precursors; the problems are about locally compositional non-uniformity, non-uniform distribution of secondary phase, and non-uniform distribution of large voids. Also, the result that the Al_2O_3 passivation layer perfectly suppressed the formation of the MoSSe layer shows a possibility of efficiency improvement through the increase of the light reflection from the Mo electrode.

Here is how to solve some of the problems at this step. First, additional NaF should be applied to compensate for the Na deficiency. In this study, it was confirmed that the distribution of Na in the thin film was different depending on the Al_2O_3 passivation area. However, since Na directly affects grain growth and can provide CZTSSe having different bulk properties, it is difficult to simply explain the change of device characteristics due to the different Na content. Thus, to verify the role of additional NaF, it is necessary to separate the factor for Na among several factors in the future work. Second, the optimized pattern using a stepper or e-beam lithography should be designed to collect the photo-generated carriers effectively. If an efficient pattern design using the e-beam process is confirmed and commercialization needs to be considered, several other alternative processes can be used, such as PDMS stamping process (nano-imprinting).

In this study, the effect of 5-nm- Al_2O_3 dot patterning on the CZTSSe solar cell efficiency was investigated. It was confirmed that the 5-nm Al_2O_3 pattern could completely inhibit MoSSe generation, and the bottom CZTSSe distribution was well controlled by dot patterning of the 5-nm- Al_2O_3 layer. However, the efficiency, J_{sc} , V_{oc} , and FF tended to decrease when the Al_2O_3 passivated area increased; the origin of the decrease in cell characteristics was expected to be inadequate Na diffusion from SLG and the insufficient optimized pattern. Nevertheless, it was found that void self-arrangement occurs,

which is of great significance in that it will be an important method to improve the local compositional non-uniformity that occurs when there is no pattern. Also, in the future work, it is necessary to apply an effective local contact structure to obtain the optical J_{SC} gain at the rear of the CZTS. When Al_2O_3 is used, $MoSe_2$ formation is prevented, and thus J_{SC} gain can be additionally expected through increased reflection from the rear surface. In addition, in order to maximize the optical reflection effect at rear surface, a new passivation layer having excellent reflection property can be applied. The structure of the solar cell applying new passivation layer that maximizes the reflection effect while the voids are arranged on the passivation layer is a new structure that has never been. This unique solar cell structure may help break the current CZTS recording efficiency.

Supplementary Materials: The following are available online at <http://www.mdpi.com/2079-4991/10/9/1874/s1>, Figure S1: Wettability of bare-Mo, BOE-etched Mo, and Al_2O_3 coated Mo; Figure S2: FESEM images of (a) top view and (b) bottom view of lifted-off CZTSSe of the sample with a passivation area of 56%; Figure S3: Lift-off process of CZTSSe cell, and Figure S4; Depth-profiles of each CZTSSe device by TOF-SIMS.

Author Contributions: Conceptualization, S.-Y.K. and S.H.; methodology, S.-H.K. and D.-H.S.; formal analysis, S.-Y.K. and S.-H.K.; investigation, S.-Y.K., S.H., Y.-I.K. and S.K.; writing—original draft preparation, S.-Y.K.; writing—review and editing, S.-Y.K., J.-K.K. and D.-H.K.; supervision, Y.-W.H., J.-K.K. and D.-H.K.; project administration, J.-K.K. and D.-H.K.; funding acquisition, J.-K.K. and D.-H.K. All authors have read and agreed to the published version of the manuscript.

Funding: This work was supported by the Korea Institute of Energy Technology Evaluation and Planning (KETEP) and the Ministry of Trade, Industry & Energy (MOTIE), Korea (No. 20173010012980). This work was also supported by the Technology Development Program to Solve Climate Change of the National Research Foundation (NRF) funded by the Ministry of Science and ICT, Korea (2016M1A2A2936781). This research was supported by the DGSIT R&D Program of the Ministry of Science and ICT of Korea (20-ET-08).

Conflicts of Interest: The authors declare no conflict of interest. The funders had no role in the design of the study; in the collection, analyses, or interpretation of data; in the writing of the manuscript, or in the decision to publish the results.

References

1. Green, M.A.; Hishikawa, Y.; Dunlop, E.D.; Levi, D.H.; Hohl-Ebinger, J.; Yoshita, M.; Ho-Baillie, A.W.Y. Solar cell efficiency tables (version 53). *Prog. Photovolt.* **2019**, *27*, 3–12. [[CrossRef](#)]
2. Powalla, M.; Paetel, S.; Ahlswede, E.; Wuerz, R.; Wessendorf, C.D.; Friedlmeier, T.M. Thin-film solar cells exceeding 22% solar cell efficiency: An overview on CuTe, Cu(In,Ga)Se₂, and perovskite based materials. *Appl. Phys. Rev.* **2018**, *5*, 041602. [[CrossRef](#)]
3. Kim, S.-Y.; Chae, W.-S.; Na, Y.-J.; Kim, S.-H.; Lee, S.; Lee, J.-H.; Heo, Y.-W. Excitation dynamics of MAPb(I_{1-x}Br_x)₃ during phase separation by photoirradiation: Evidence of sink, band filling, and Br-rich phase coarsening. *J. Alloys Compd.* **2019**, *806*, 1180–1187. [[CrossRef](#)]
4. Kim, S.-Y.; Lee, S.; Chae, W.-S.; Lee, J.-H.; Heo, Y.-W. Real time observation of photo-instability of ternary-halide mixed CH₃NH₃Pb(Br_{1-x-y}Cl_xI_y)₃ perovskite: Preferential diffusion of small halide ions. *J. Alloys Compd.* **2019**, *808*, 151716. [[CrossRef](#)]
5. Cho, H.; Kim, Y.-H.; Wolf, C.; Lee, H.-D.; Lee, T.-W. Improving the stability of Metal Halide perovskite Materials and Light-Emitting Diodes. *Adv. Mater.* **2018**, *30*, 1704587. [[CrossRef](#)] [[PubMed](#)]
6. Hong, M.J.; Svadlenak, S.R.; Goulas, K.A.; Labram, J.G. Thermal stability of mobility in methylammonium lead iodide. *J. Phys. Mater.* **2020**, *3*, 014003. [[CrossRef](#)]
7. Ava, T.T.; Mamun, A.A.; Marsillac, S.; Namkoong, G. A Review: Thermal Stability of Methylammonium Lead Halide Based Perovskite Solar Cells. *Appl. Sci.* **2019**, *9*, 188. [[CrossRef](#)]
8. Seol, J.-S.; Lee, S.-Y.; Lee, J.-C.; Nam, H.-D.; Kim, K.-H. Electrical and optical properties of Cu₂ZnSnS₄ thin films prepared by rf magnetron sputtering process. *Sol. Energy Mater. Sol. Cells* **2003**, *75*, 155–162. [[CrossRef](#)]
9. Walsh, A.; Chen, S.; Wei, S.-H.; Gong, X.-G. Kesterite Thin-Film Solar Cells: Advances in Materials Modelling of Cu₂ZnSnS₄. *Adv. Energy Mater.* **2012**, *2*, 400–409. [[CrossRef](#)]
10. Wang, W.; Winkler, M.T.; Gunawan, O.; Gokmen, T.; Todorov, T.K.; Zhu, Y.; Mitzi, D.B. Device Characteristics of CZTSSe Thin-Film Solar Cells with 12.6% Efficiency. *Adv. Energy Mater.* **2014**, *4*, 1301465. [[CrossRef](#)]

11. Chen, S.; Walsh, A.; Yang, J.-H.; Gong, X.G.; Sun, L.; Yang, P.-X.; Chu, J.-H.; Wei, S.-H. Compositional dependence of structural and electronic properties of $\text{Cu}_2\text{ZnSn}(\text{S,Se})_4$ alloys for thin film solar cells. *Phys. Rev. B* **2011**, *83*, 125201. [[CrossRef](#)]
12. Gokmen, T.; Gunawan, O.; Todorov, T.K.; Mitzi, D.B. Band tailing and efficiency limitation in kesterite solar cells. *Appl. Phys. Lett.* **2013**, *103*, 103506. [[CrossRef](#)]
13. Scragg, J.J.S.; Larsen, J.K.; Kumar, M.; Persson, C.; Sendler, J.; Siebentritt, S.; Bjorkman, C.P. Cu-Zn disorder and band gap fluctuations in $\text{Cu}_2\text{ZnSn}(\text{S,Se})_4$: Theoretical and experimental investigations. *Phys. Status Solidi B* **2016**, *253*, 247–254. [[CrossRef](#)]
14. Nam, D.; Cho, S.; Sim, J.-H.; Yang, K.-J.; Son, D.-H.; Kim, D.-H.; Kang, J.-K.; Kwon, M.-S.; Jeon, C.-W.; Cheong, H. Solar conversion efficiency and distribution of ZnS secondary phase in $\text{Cu}_2\text{ZnSnS}_4$ solar cells. *Sol. Energy Mater. Sol. Cells* **2016**, *149*, 226–231. [[CrossRef](#)]
15. Kim, S.-Y.; Son, D.-H.; Kim, Y.-I.; Kim, S.-H.; Kim, S.; Ahn, K.; Sung, S.-J.; Hwang, D.-K.; Yang, K.-J.; Kang, J.-K.; et al. Void and Secondary phase formation mechanisms of CZTSSe using Sn/Cu/Zn/Mo stacked elemental precursors. *Nano Energy* **2019**, *59*, 399–411. [[CrossRef](#)]
16. Hernández-Martínez, A.; Placidi, M.; Arqués, L.; Giraldo, S.; Sánchez, Y.; Izquierdo-Roca, V.; Pistor, P.; Valentini, M.; Malerba, C.; Saucedo, E. Insights into the Formation Pathways of $\text{Cu}_2\text{ZnSnSe}_4$ Using Rapid Thermal Processes. *ACS Appl. Energy Mater.* **2018**, *1*, 1981–1989. [[CrossRef](#)]
17. Schorr, S.; Gurieva, G.; Guc, M.; Dimitrievska, M.; Pérez-Rodríguez, A.; Izquierdo-Roca, V.; Schnohr, C.S.; Kim, J.; Jo, W.; Merino, J.M. Point defects, compositional fluctuations, and secondary phases in non-stoichiometric kesterites. *J. Phys. Energy* **2020**, *2*, 012002. [[CrossRef](#)]
18. Giraldo, S.; Jehl, Z.; Placidi, M.; Izquierdo-Roca, V.; Pérez-Rodríguez, A.; Saucedo, E. Progress and Perspectives of Thin Film Kesterite Photovoltaic Technology: A Critical Review. *Adv. Mater.* **2019**, *31*, 1806692. [[CrossRef](#)]
19. Li, J.; Yuan, Z.-K.; Chen, S.; Gong, X.-G.; Wei, S.-H. Effective and Noneffective Recombination Center Defects in $\text{Cu}_2\text{ZnSnS}_4$: Significant Difference in Carrier Capture Cross Sections. *Chem. Mater.* **2019**, *31*, 826–833. [[CrossRef](#)]
20. Kim, S.; Park, J.-S.; Walsh, A. Identification of Killer Defects in Kesterite Thin-Film Solar Cells. *ACS Energy Lett.* **2018**, *3*, 496–500. [[CrossRef](#)]
21. Weber, W.; Mainz, R.; Schock, H.W. On the Sn loss from this films of the material system Cu-Zn-Sn-S in high vacuum. *J. Appl. Phys.* **2010**, *107*, 013516. [[CrossRef](#)]
22. Redinger, A.; Berg, D.M.; Dale, P.J.; Siebentritt, S. The consequences of Kesterite Equilibria for Efficient Solar Cells. *J. Am. Chem. Soc.* **2011**, *133*, 3320–3323. [[CrossRef](#)] [[PubMed](#)]
23. Son, D.-H.; Kim, S.-H.; Kim, S.-Y.; Kim, Y.-I.; Sim, J.-H.; Park, S.-N.; Jeon, D.-H.; Hwang, D.-K.; Sung, S.-J.; Kang, J.-K.; et al. Effect of soild- H_2S gas reaction on CZTSSe thin film growth and photovoltaic properties of a 12.62% efficiency device. *J. Mater. Chem. A* **2019**, *44*, 25279–258289. [[CrossRef](#)]
24. Ahn, K.; Kim, S.-Y.; Kim, S.; Son, D.-H.; Kim, S.-H.; Kim, S.Y.; Kim, J.; Sung, S.-J.; Kim, D.-H.; Kang, J.-K. Flexible high-efficiency CZTSSe solar cells on stainless steel substrates. *J. Mater. Chem. A* **2019**, *43*, 24891–24899. [[CrossRef](#)]
25. Yang, K.-J.; Kim, S.; Kim, S.-Y.; Ahn, K.; Son, D.-H.; Kim, S.-H.; Lee, S.-J.; Kim, Y.-I.; Park, S.-N.; Sung, S.-J.; et al. Flexible $\text{Cu}_2\text{ZnSn}(\text{S,Se})_4$ solar cells with over 10% efficiency and methods of enlarging the cell area. *Nat. Commun.* **2019**, *10*, 2959. [[CrossRef](#)] [[PubMed](#)]
26. Hong, S.; Kim, S.-Y.; Son, D.-H.; Kim, S.-H.; Kim, Y.-I.; Yang, K.-J.; Heo, Y.-W.; Kang, J.-K.; Kim, D.-H. Self-Alignment of Bottom CZTSSe by Patterning of an Al_2O_3 Intermediate Layer. *Nanomaterials* **2020**, *10*, 43. [[CrossRef](#)]
27. Yan, C.; Huang, J.; Sun, K.; Johnston, S.; Zhang, Y.; Sun, H.; Pu, A.; He, M.; Liu, F.; Eder, K.; et al. $\text{Cu}_2\text{ZnSnS}_4$ solar cells with over 10% power conversion efficiency enabled by heterojunction heat treatment. *Nat. Energy* **2018**, *3*, 764–772. [[CrossRef](#)]
28. Giraldo, S.; Saucedo, E.; Neuschitzer, M.; Oliva, F.; Placidi, M.; Alcobé, X.; Izquierdo-Roca, V.; Kim, S.; Tampo, H.; Shibata, H.; et al. How small amounts of Ge modify the formation pathways and crystallization of kesterites. *Energy Environ. Sci.* **2018**, *11*, 582. [[CrossRef](#)]
29. Kim, S.-Y.; Kim, S.-H.; Hong, S.; Son, D.-H.; Kim, Y.-I.; Kim, S.; Ahn, K.; Yang, K.-J.; Kim, D.-H.; Kang, J.-K. Secondary Phase Formation Mechanism in the Mo-Back Contact Region during Sulfo-Selenization Using a Metal Precursor: Effect of Wettability between a Liquid Metal and Substrate on Secondary Phase Formation. *ACS Appl. Mater. Interfaces* **2019**, *11*, 23160–23167. [[CrossRef](#)]

30. Vermang, B.; Fjällström, V.; Pettersson, J.; Salomé, P.; Edorff, M. Development of rear surface passivated Cu(In,Ga)Se₂ thin film solar cells with nano-sized local rear point contacts. *Sol. Energy Mater. Sol. Cells* **2013**, *117*, 505–511. [[CrossRef](#)]
31. Vermang, B.; Wätjen, J.T.; Fjällström, V.; Rostvall, F.; Edoff, M.; Kotipalli, R.; Henry, F.; Flandre, D. Employing Si solar cell technology to increase efficiency of ultra-thin Cu(In,Ga)Se₂ solar cells. *Prog. Photovolt.* **2014**, *22*, 1023–1029. [[CrossRef](#)] [[PubMed](#)]
32. Kim, J.; Park, S.; Ryu, S.; Oh, J.; Shin, B. Improving the open-circuit voltage of Cu₂ZnSnSe₄ thin film solar cells via interface passivation. *Prog. Photovolt. Res. Appl.* **2017**, *25*, 308–317. [[CrossRef](#)]
33. Kim, S.-Y.; Son, D.-H.; Kim, S.-H.; Kim, Y.-I.; Kim, S.; Ahn, K.; Yang, K.-J.; Kang, J.-K.; Kim, D.-H. Effect of Cu–Sn–Se Liquid Phase on Grain Growth and Efficiency of CZTSSe Solar Cells. *Adv. Energy Mater.* **2020**, *10*, 1903173. [[CrossRef](#)]
34. Vermang, B.; Fjällström, V.; Gao, X.; Edoff, M. Improved Rear Surface Passivation of Cu (In,Ga)Se₂ Solar Cells: A Combination of an Al₂O₃ Rear Surface Passivation Layer and Nanosized Local Rear Point Contacts. *IEEE J. Photovolt.* **2014**, *4*, 486–492. [[CrossRef](#)]
35. Johnson, M.; Baryshev, S.V.; Thimsen, E.; Manno, M.; Zhang, X.; Veryovkin, I.V.; Leighton, C.; Aydil, E.S. Alkali-metal-enhanced grain growth in Cu₂ZnSnS₄ thin films. *Energy Environ. Sci.* **2014**, *7*, 1931. [[CrossRef](#)]
36. Gershon, T.; Shin, B.; Bojarczuk, N.; Hopstaken, M.; Mitzi, D.B.; Guha, S. The Role of Sodium as a Surfactant and Suppressor of Non-Radiative Recombination at Internal Surfaces in Cu₂ZnSnS₄. *Adv. Energy Mater.* **2015**, *5*, 1400849. [[CrossRef](#)]
37. Wang, D.; Chen, J.; Wu, M.; Gao, S.; Wu, L.; Ao, J.; Sun, Y.; Zhang, Y. Synergistic effect of Na and Se on CZTSe solar cells through a soft chemical process. *Sol. Energy Mater. Sol. Cells* **2019**, *198*, 35–43. [[CrossRef](#)]
38. Yang, K.-J.; Sim, J.-H.; Jeon, B.; Son, D.-H.; Kim, D.-H.; Sung, S.-J.; Hwang, D.-K.; Song, S.; Khadka, D.B.; Kim, J.; et al. Effects of Na and MoS₂ on Cu₂ZnSnS₄ thin-film solar cell. *Prog. Photovolt.* **2015**, *23*, 862–873. [[CrossRef](#)]
39. Li, J.B.; Chawla, V.; Clemens, B.M. Investigating the Role of Grain Boundaries in CZTS and CZTSSe Thin Film Solar Cells with Scanning Probe Microscopy. *Adv. Mater.* **2012**, *24*, 720–723. [[CrossRef](#)]
40. Liu, C.Y.; Li, Z.M.; Gu, H.Y.; Chen, S.Y.; Xiang, H.; Gong, X.G. Sodium Passivation of the Grain Boundaries in CuInSe₂ and Cu₂ZnSnS₄ for High-Efficiency Solar Cells. *Adv. Energy Mater.* **2017**, *7*, 1601457. [[CrossRef](#)]
41. Prabhakar, T.; Jampan, N. Effect of sodium diffusion on the structural and electrical properties of Cu₂ZnSnS₄ thin films. *Sol. Energy Mater. Sol. Cells* **2011**, *95*, 1001–1004. [[CrossRef](#)]
42. Tampo, H.; Kim, K.M.; Kim, S.; Shibata, H.; Niki, S. Improvement of minority carrier lifetime and conversion efficiency by Na incorporation in Cu₂ZnSnSe₄ solar cells. *J. Appl. Phys.* **2017**, *122*, 023106. [[CrossRef](#)]
43. Gershon, T.; Lee, Y.S.; Mankad, R.; Gunawan, O.; Gokmen, T.; Bishop, D.; McCandless, B.; Guha, S. The impact of sodium on the sub-bandgap states in CZTSe and CZTS. *Appl. Phys. Lett.* **2015**, *106*, 123905. [[CrossRef](#)]
44. Ledinek, D.; Keller, J.; Hägglund, C.; Chen, W.-C.; Edoff, M. Effect of NaF pre-cursor on alumina and hafnia rear contact passivation layers in ultra-thin Cu (In,Ga)Se₂ solar cells. *Thin Solid Films* **2019**, *683*, 156–164. [[CrossRef](#)]
45. Casper, P.; Hünig, R.; Gomard, G.; Kiowski, O.; Reitz, C.; Lemmer, U.; Powalla, M.; Hetterich, M. Optoelectrical improvement of ultra-thin Cu(In,Ga)Se₂ solar cells through microstructured MgF₂ and Al₂O₃ back contact passivation layer. *Phys. Status Solidi RRL* **2016**, *10*, 376–380. [[CrossRef](#)]
46. Hages, C.J.; Redinger, A.; Levchenko, S.; Hempel, H.; Koeper, M.J.; Agrawal, R.; Greiner, D.; Kaufmann, C.A.; Unold, T. Identifying the Real Minority Carrier Lifetime in Nonideal Semiconductors: A Case Study of Kesterite Materials. *Adv. Energy Mater.* **2017**, *7*, 1700167. [[CrossRef](#)]
47. Courel, M.; Andrade-Arvizu, J.A.; Vigil-Galán, O. The role of buffer/kesterite interface recombination and minority carrier lifetime on kesterite thin film solar cells. *Mater. Res. Express* **2016**, *3*, 095501. [[CrossRef](#)]
48. Gunawan, O.; Pae, S.R.; Bishop, D.M.; Virgus, Y.; Noh, J.H.; Jeon, N.J.; Lee, Y.S.; Shao, X.; Todorov, T.; Mitzi, D.B.; et al. Carrier-resolved photo-Hall effect. *Nature* **2019**, *575*, 151–155. [[CrossRef](#)]

